ADVANCING EARTH AND SPACE SCIENCES

JGR Atmospheres

RESEARCH ARTICLE
10.1029/2023JD040230

Contribution of Recycled and External Advected Moisture to Precipitation and Its Inter-Annual Variation Over the Tibetan Plateau

Mengnan Ma[1,2], Jianping Tang[1,2], Tinghai Ou[3], and Deliang Chen[3]

[1]Key Laboratory of Mesoscale Severe Weather/Ministry of Education, Nanjing University, Nanjing, China, [2]School of Atmospheric Sciences, Nanjing University, Nanjing, China, [3]Department of Earth Sciences, Regional Climate Group, University of Gothenburg, Gothenburg, Sweden

Key Points:

- Precipitation recycling ratio (PRR) over the Tibetan Plateau exhibits significant variations both with elevation and from year to year
- The inter-annual variation of precipitation is strongly influenced by the net influx of water vapor and associated atmospheric circulations
- Inter-annual variation in PRR is significantly influenced by the inflow of water vapor and wind strength, especially during colder seasons

Supporting Information:

Supporting Information may be found in the online version of this article.

Correspondence to:

J. Tang,
jptang@nju.edu.cn

Citation:

Ma, M., Tang, J., Ou, T., & Chen, D. (2024). Contribution of recycled and external advected moisture to precipitation and its inter-annual variation over the Tibetan Plateau. *Journal of Geophysical Research: Atmospheres*, *129*, e2023JD040230. https://doi.org/10.1029/2023JD040230

Received 16 OCT 2023
Accepted 30 APR 2024

Abstract

In this study, we performed a high-resolution simulation using the Weather Research and Forecasting model, integrated with water vapor tracers, covering the years 2005–2019. Our objective was to obtain deeper insights into the spatiotemporal dynamics of external advected and local evaporative water vapor, and to elucidate their impact on precipitation patterns across the Tibetan Plateau (TP). Our findings underscore that a significant proportion of TP's precipitation originates from external advected water vapor, primarily entering through the western and southern boundaries. During summer, stronger zonal and meridional water vapor transport, driven by prevailing westerly winds and the Asian monsoon, significantly influences seasonal and spatial precipitation variations. Additionally, we observed that the inter-annual variation of precipitation is intricately linked to changes in the net water vapor influx, modulated by alterations in atmospheric circulation. We also analyze the Precipitation Recycling Ratio (PRR) which refers to the proportion of precipitation originated from local evaporative water vapor to the total precipitation, revealing distinctive elevation-dependent variations aligned with grassland distribution. Notably, PRR exhibits asynchronous shifts with precipitation at different timescales, potentially linked to soil moisture-precipitation feedback at intra-annual scales. Moreover, the investigation highlights that inter-annual variations in PRR are primarily linked to the inflow and outflow of water vapor as well as wind strength at 500 hPa, particularly prominent during colder seasons, while thermal factors carry comparable weight to dynamical factors in warmer seasons.

Plain Language Summary

Precipitation constitutes a vital component of the complex climatic conditions as well as the hydrological cycle over the Tibetan Plateau (TP), known as the “Asian Water Tower.” Its distinct spatiotemporal variations, closely tied to the advected water vapor from external areas as well as evaporated within the TP, have direct impacts on local ecosystem and downstream water supply. These effects have profound socio-economic and environmental consequences. In this study, we found that temporal variations and spatial inhomogeneities in precipitation are primarily impacted by the advection of external water vapor, mainly through atmospheric circulation. Additionally, about 18.9% of the annual precipitation stems from local evaporation, as indicated by the precipitation recycling ratio, which reflects the strength of regional land-atmospheric interactions. Precipitation recycling processes are likely influenced by precipitation through soil moisture at intra-annual timescale, but are notably impacted by the inflow of water vapor and wind strength at inter-annual timescale. These results provide valuable insights into understanding precipitation variations at different spatiotemporal scales and contribute to more effective water resources management over the TP.

1. Introduction

Known as the “Asian Water Tower”, the Tibetan Plateau (TP) holds a pivotal role in regulating Asia's water cycle (Immerzeel et al., 2010; X. Xu et al., 2008). It serves as the source region for several major Asian rivers, including the Brahmaputra, Ganges, Indus, Yellow, and Yangtze (Chao et al., 2017; Gao et al., 2019; L. Zhang et al., 2013), supplying water to nearly 2 billion residents (Liu et al., 2020; Qu et al., 2019; Yao et al., 2022). Consequently, a profound understanding of the hydrological cycle dynamics holds paramount importance (Ma et al., 2018). Precipitation serves as a pivotal element in the hydrological cycle (Curio & Scherer, 2016; Yao, Qin, et al., 2013) and a key component of regional water resources (Buytaert et al., 2010; Cuo & Zhang, 2017; Jia et al., 2017). Changes in the contributions of moisture to precipitation impact the regional climate, hydrological cycle, and water reserves, especially under the background of ongoing global changes (Ciric et al., 2018; Z. Li et al., 2019; X. Li et al., 2022; Liu et al., 2015).

Generally, terrestrial precipitation originates from two primary sources: (a) water vapor evaporated outside the region and transported in, and (b) water vapor evaporated within the region (Brubaker et al., 1993). Numerous studies have demonstrated that moisture transported to the TP primarily originates from the Indian summer monsoon and the westerlies (B. Chen et al., 2012; Feng & Zhou, 2012; C. Zhang et al., 2019).

In the last several years, increased attention has been dedicated to understanding the role of atmospheric moisture transport and its internal physical mechanisms affecting TP's precipitation (Cannon et al., 2017; Curio et al., 2015; Dong et al., 2016; Wang et al., 2017). Utilizing the High Asia Refined analysis (HAR; Maussion et al., 2014), Curio et al. (2015) measured moisture transport across 14 specified boundaries of the TP, highlighting valleys in the Himalayas as facilitators of moisture transport to the inner TP. Conversely, no significant transport from the East Asian monsoon was observed. Using convection-permitting model (CPM) with similar boundary definitions, Zhao et al. (2021) identified that primary entries for external water vapor into the TP are the western and southern boundaries while the eastern boundary functions as the major exit. The added value of CPM in reducing the wet bias is achieved by generating stronger outflow through the eastern boundary. However, previous literature either utilized global reanalysis data sets to measure the transport or focused on single season/year due to the expensive computational cost of conducting high-resolution numerical simulation, preventing from obtaining spatiotemporal details of water vapor transport (WVTP) climatology and its inter-annual variations. On the other hand, contribution of local evaporation to precipitation serves as an essential measure of a region's capability to replenish its water supplies (Juan et al., 2022) and plays a fundamental role in sustaining the dynamics of hydrological processes (An et al., 2017). The contribution of local evaporation to local precipitation is referred to as precipitation recycling (Trenberth, 1999). Previous literature have characterized the precipitation recycling ratio (PRR) as the fraction of precipitation stemming from locally evaporative water vapor relative to the total precipitation (Brubaker et al., 1993; Eltahir & Bras, 1994, 1996). The application of diverse data sets with different data sources and methodologies could result in significant discrepancies in the estimated PRR across current literature. For instance, for the whole TP, C. Zhang et al. (2017) showed that the PRR is about 18% using the Euler-based water vapor tracing method, while Curio et al. (2015) estimated the PRR as about 63% through the analysis of water balance. For the subregions of the TP, estimated PRR is about 35% over the southeastern TP based on Lagrange-based backward water vapor tracing method (Y. Xu & Gao, 2019) but about 25.8% over the northern TP by applying a Eulerian framework (Pan et al., 2019). Therefore, the PRR and its interannual variation over the TP, remains uncertain (Zhao & Zhou, 2021). These facts underscore the necessity for enhanced modeling-based knowledge about both large-scale and local-scale atmospheric processes regulating the TP's hydrological cycle (Yao, Masson-Delmotte, et al., 2013).

In understanding the vital role of moisture sources in water cycles, diverse numerical methods have been devised to quantitatively identify these sources over and around the TP. These methods encompass analytical, Lagrangian and Eulerian models (e.g., Dominguez et al., 2006; Insua-Costa & Miguez-Macho, 2018; Stohl & James, 2004, 2005). Analytical models offer a computationally efficient means to estimate the proportion of recycled precipitation to total precipitation within a specific area (Burde & Zangvil, 2001a, 2001b). However, relying on assumptions that the atmospheric column is well-mixed and the alteration in atmospheric moisture storage is relatively insignificant compared to other terms in the mass balance equation at monthly or longer time scales (Dominguez et al., 2006), these models generally offer a preliminary estimation of the PRR, compromising their precision and applicability (Bosilovich, 2002).

Lagrangian models, builted upon the tracking of individual fluid particles in both space and time, have gained popularity in diagnosing moisture transport and determining moisture origins (Brubaker et al., 2001; Gimeno et al., 2010; James et al., 2004). Their advantages encompass computational efficiency and the ability to trace particles back in time without a priori selection of source regions (B. Chen et al., 2019; Dirmeyer & Brubaker, 2006; Huang et al., 2018). Nevertheless, notable biases can arise due to simplifications in their formulation (e.g., neglecting phase changes along the parcels' paths) and gradual increase in the uncertainty of air parcel trajectories (Stohl, 1998).

Eulerian models, often referred to as water vapor tracers (WVTs), account for both grid-scale and parameterization-solved physical processes affecting atmospheric moisture, making them highly accurate for studying precipitation recycling (Insua-Costa & Miguez-Macho, 2018). Typically, they couple moisture tracing technique with global or mesoscale climate models (Eiras-Barca et al., 2017; Singh et al., 2016), linking biases in WVTs closely to the performance of their coupled models. However, these models entail significantly higher computational costs compared to other mentioned techniques, especially at higher resolutions (Dominguez et al., 2022). Other physical moisture tracing techniques encompass analyzing the isotopic composition of precipitation (Cai & Tian, 2016; Guo et al., 2017). A comprehensive review of various moisture tracing techniques can be found in Gimeno et al. (2012) and Gimeno Presa et al. (2020). To date, considering the promising prospect of WVTs, they have been incorporated in different global climate models (Koster et al., 1986; Numaguti, 1999; Werner et al., 2001) and regional climate models (RCMs; Knoche & Kunstmann, 2013; Gao et al., 2020; Sodemann et al., 2009) which can enhance the depiction of hydrological cycle's small-scale characteristics. Though WVTs are believed to be helpful in regional climate research, given the current progress and findings, the exploration of Euler-based techniques over the TP is still in its initial phase. The follow-up studies are in great demand of (a) higher spatial resolution to more faithfully represent sub-grid physical processes and (b) decadal-long temporal coverage to reflect climatic characteristic, as well as capture inter-annual variation features.

Here, we employ WVTs integrated into the Weather Research and Forecasting (WRF) model to quantitatively assess contributions of remote WVTP and local moisture recycling to precipitation. We also investigate their roles in influencing inter-annual variations in precipitation and present an overarching overview of the water cycle climatology. The paper is organized as follows: Section 2 outlines the application of the WVT technique, experimental design, data sources, and methods used. In Section 3, we assess the WRF simulation of precipitation. Section 4 analyzes the external WVTP and local precipitation recycling. Finally, Section 5 encapsulates our conclusions and findings.

2. Model, Data, and Methodology

2.1. WRF-WVT Description

In this study, WVTs have been included within the framework of WRF model (WRF-WVT hereafter). WRF-WVT enables the tracing of moisture originated as evapotranspiration from a predefined region (Dominguez et al., 2016). The tracer is numerically handled samely as simulated moisture, with the exception of its origins, which are confined to specified regions of interest. The moisture tagging technique is founded on replicating the prognostic equation for total moisture to model moisture tracers:

$$\frac{\partial q_n}{\partial t} = -v \cdot \nabla q_n + v_q \cdot \nabla^2 q_n + \left(\frac{\partial q_n}{\partial t}\right)_{\text{PBL}} + \left(\frac{\partial q_n}{\partial t}\right)_{\text{microphysics}} + \left(\frac{\partial q_n}{\partial t}\right)_{\text{convection}} \tag{1}$$

where q_n represents the various moisture species including water vapor, cloud water, rain water, snow, ice and graupel. $-v \cdot \nabla q_n$ and $v_q \cdot \nabla^2 q_n$ refer to the tendencies caused by advection and molecular diffusion, respectively. $\left(\frac{\partial q_n}{\partial t}\right)_{\text{PBL}}$, $\left(\frac{\partial q_n}{\partial t}\right)_{\text{microphysics}}$ and $\left(\frac{\partial q_n}{\partial t}\right)_{\text{convection}}$ represent subgrid physical processes influencing atmospheric moisture (e.g., phase transitions, precipitation, or redistribution due to turbulent diffusion and convection). The traced moisture replicates all the moisture processes depicted in WRF, and consequently, several variables tq_n are additionally created in accordance with the moisture tracers: *tvapor, tcloud, train, tsnow, tice,* and *tgraupel*.

The WVT technique facilitates the tracing of moisture from sources in either two or three dimensions. Typically, a two-dimensional source involves tagging surface evapotranspiration from a specific region. A three-dimensional source can encompass the whole atmosphere over an area of interest, including the water vapor evaporated and advected into the region, or to only a part of it (e.g., the stratosphere). For more thorough explanations, see Insua-Costa and Miguez-Macho (2018).

In this study, the WRF model version 4.3.3 (Skamarock et al., 2019) with 9 km horizontal resolution and forty hybrid-sigma levels is used. The model top is set at 50 hPa. The simulation domain is illustrated in Figure 1, configured with 391 (571) grid points oriented north–south (east–west). In WVT method, the Yonsei University planetary boundary layer (PBL) scheme (Hong et al., 2006) and the WRF Single-Moment 6-class (WSM6) microphysics scheme (Hong & Lim, 2006) have been adjusted to calculate the related tracer moisture tendencies due to their direct effect on moisture dynamics, and thus are essential to enable WVT implementations. The rest of the parameterizations selected include the rapid radiative transfer model-global shortwave and longwave radiation schemes (Iacono et al., 2008) and the Noah land surface model (F. Chen & Dudhia, 2001). Tracers can also

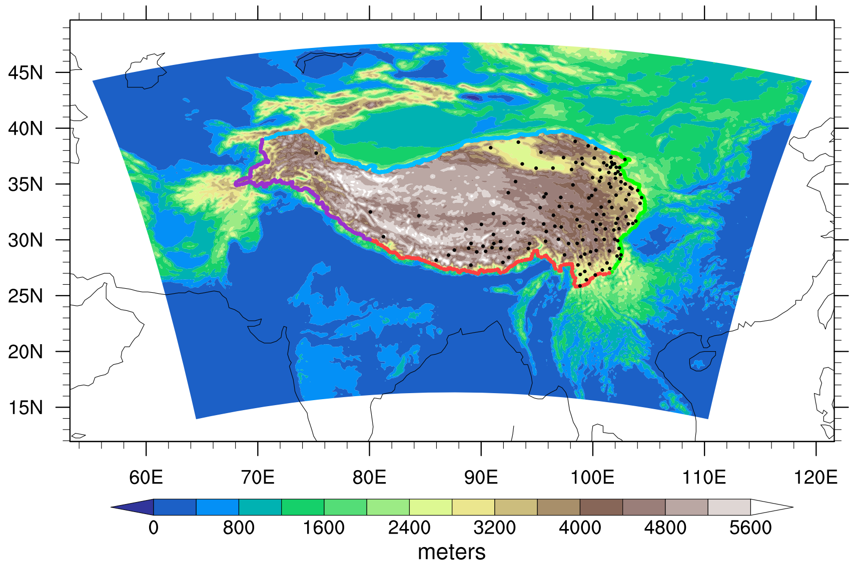

Figure 1. Simulation domain (shaded) of WRF-WVT, with the southern, western, northern, and eastern boundaries of the Tibetan Plateau indicated by red, purple, blue and green polylines. Black dots mark the locations of meteorological stations. The color bar indicates the elevation (m).

be utilized at the convection-permitting scale, thus, no cumulus parameterization is used here (Ma et al., 2021, 2023a, 2023b; Ou et al., 2023; Zhou et al., 2023).

Utilizing the fifth generation Global Reanalysis data (ERA5) with spatial resolution of 0.25° × 0.25° and temporal resolution of 3-hr (Hersbach et al., 2020), a 15-year WRF-WVT simulation spanning from 2005 to 2019 is conducted within the geographical domain illustrated in Figure 1. This simulation encompasses 15 consecutive annual runs. Each run starts in November 20 of the previous year with a spin-up of more than 1 month and ends in December 31 of the simulating year, with the simulation results from January 1 to December 31 used for annual analysis. Results from 15 spring (March–May, 2005–2019), summer (June–August, 2005–2019), autumn (September-November, 2005–2019) and 14 winter (December-January-February, 2005/2006–2018/2019) seasons are also taken into analysis. In this study, WRF-WVT tags the local evaporation (two-dimensional source) over the TP, and the external advected water vapor (out of TP; three-dimensional source) can be derived by excluding the local evaporated water vapor from the total water vapor.

2.2. Observational Data Sets

Observations used in evaluating simulated precipitation include the daily in situ observation from 144 stations over the TP (Figure 1), the Integrated Multi-satellitE Retrievals for the Global Precipitation Measurement mission (IMERG; Huffman et al., 2020) products, and the newly released high-resolution precipitation production TPHiPr (Jiang et al., 2023). The meteorological stations exhibit uneven distribution across the TP, and are sparsely distributed especially over the central and western TP. As supplementary, IMERG, with temporal resolution of half an hour and spatial resolution of 0.1°, is also employed. Tan et al. (2017) have emphasized the widespread application of IMERG, ranging from the analysis of precipitation features to its utility in hydrological research to the assessment of weather and climate models. Another gridded data set, TPHiPr, is produced by combining the atmospheric simulation-based downscaling of ERA5 using a convolution neural network based model (ERA5_CNN) with records from over 9,000 rain gauges. TPHiPr offers precipitation data spanning from 1979 to 2020 at 3 km spatial resolution and hourly temporal resolution, and retains the general spatial patterns of precipitation from ERA5_CNN, with diminished wet biases and more spatially homogeneous accuracy. The outputs of the WRF model are converted to the station sites and 0.1° × 0.1° grid points using the inverse distance squared weighting interpolation method to compare with station observation and gridded data sets (IMERG and TPHiPr), respectively.

2.3. Methods

The vertically integrated water vapor fluxes and net water vapor fluxes are calculated as:

$$\mathrm{FQU} = \int_{sfc}^{toa} \frac{qu}{g} dp \tag{2}$$

$$\mathrm{FQV} = \int_{sfc}^{toa} \frac{qv}{g} dp \tag{3}$$

$$\mathrm{Flow} = \oint_{tp} \mathrm{FQU\ dy} + \mathrm{FQV\ dx} \tag{4}$$

Where q, u and v represent specific humidity, zonal and meridional wind speed; FQU and FQV represent the zonal and meridional water vapor flux; Flow represents the inflow and outflow of water vapor, which is calculated along the polylines enclosing the entire TP, and is denoted by positive and negative values, respectively. The total of both positive and negative values of Flow denotes the net income of water vapor, which is a key component of the atmospheric water resources. The Flow values are also summed along the four boundaries of TP (Figure 1) that are defined generally following that in Y. Li et al. (2022) and Yan et al. (2020), in order to acquire an estimation of the relative importance of WVTP channel.

3. Validation of WRF-WVT's Precipitation

Figure 2 exhibits the spatial pattern of biases in annual, summer and winter mean daily precipitation compared with station records (Figures 2a–2c) and gridded data set (Figures 2d–2i), respectively, as well as the seasonal cycle (Figures 2j and 2k) and inter-annual variation (Figures 2l and 2m) of precipitation from WRF-WVT and different observational data sets. Compared with both in situ and gridded observations, it is clear that WRF-WVT can successfully capture the spatial pattern of annual and seasonal mean precipitation, with spatial correlation coefficients above 0.73 (significant at the 99% confidence level). Consistent wet biases are detected mainly over the southeastern and northwestern TP, probably due to the more intensified upward motion (Figure S1 in Supporting Information S1), and dry biases are found over the northern and central TP especially in summer, which is associated with reduced total column water vapor (Figure S2 in Supporting Information S1). Generally, comparison results are in good agreement between different observational data sets except slight discrepancies for summer mean precipitation, with the dry biases more widespread when compared against TPHiPr.

Apart from the climatology of annual and seasonal mean precipitation, WRF-WVT also effectively reproduces the seasonal cycle of precipitation which peaks in July. With regard to the inter-annual variation of precipitation, the temporal correlation coefficients (TCCs) between WRF-WVT and station observations, IMERG and TPHiPr are 0.74, 0.86 and 0.78 (significant at the 99% confidence level), respectively. These indicate WRF-WVT's reliability over the TP in realistically depicting the intra- and inter-annual variation of precipitation. The evaluation presented above give further confidence in carrying out precipitation tracing analysis over the TP with WRF-WVT.

4. Contribution of Recycled and External Advected Water Vapor

4.1. Precipitation From Local and Non-Local Origin

As generally acknowledged, precipitation over the TP is the combination of water vapor from advection and local evaporative water vapor, but their quantification has been highly controversial. Figure 3 displays the spatial pattern of 15-year averaged annual and seasonal mean fraction of traced precipitation to total precipitation. Specifically, tracer precipitation with local origin is related to local evaporation, and can reflect the regional land-atmospheric interactions, while that with non-local region is associated with external water vapor flux forcing. According to the WRF-WVT, PRR is higher over the central-eastern TP, but lower over the western TP. The annual mean PRR is about 18.9% when averaged over the TP, which aligns well with previous studies using the Euler-based model, such as 18% in C. Zhang et al. (2019) and around 20% in Gao et al. (2020), as well as studies using bulk models, such as 20.8% in Guo et al. (2018). In addition, substantial seasonal variation of PRR is found, which is about 23.3% in summer but decreases to about 12.7% in winter, highlighting the importance of local evaporation (external advected water vapor) to the total precipitation in summer (winter). Therefore, when

10.1029/2023JD040230

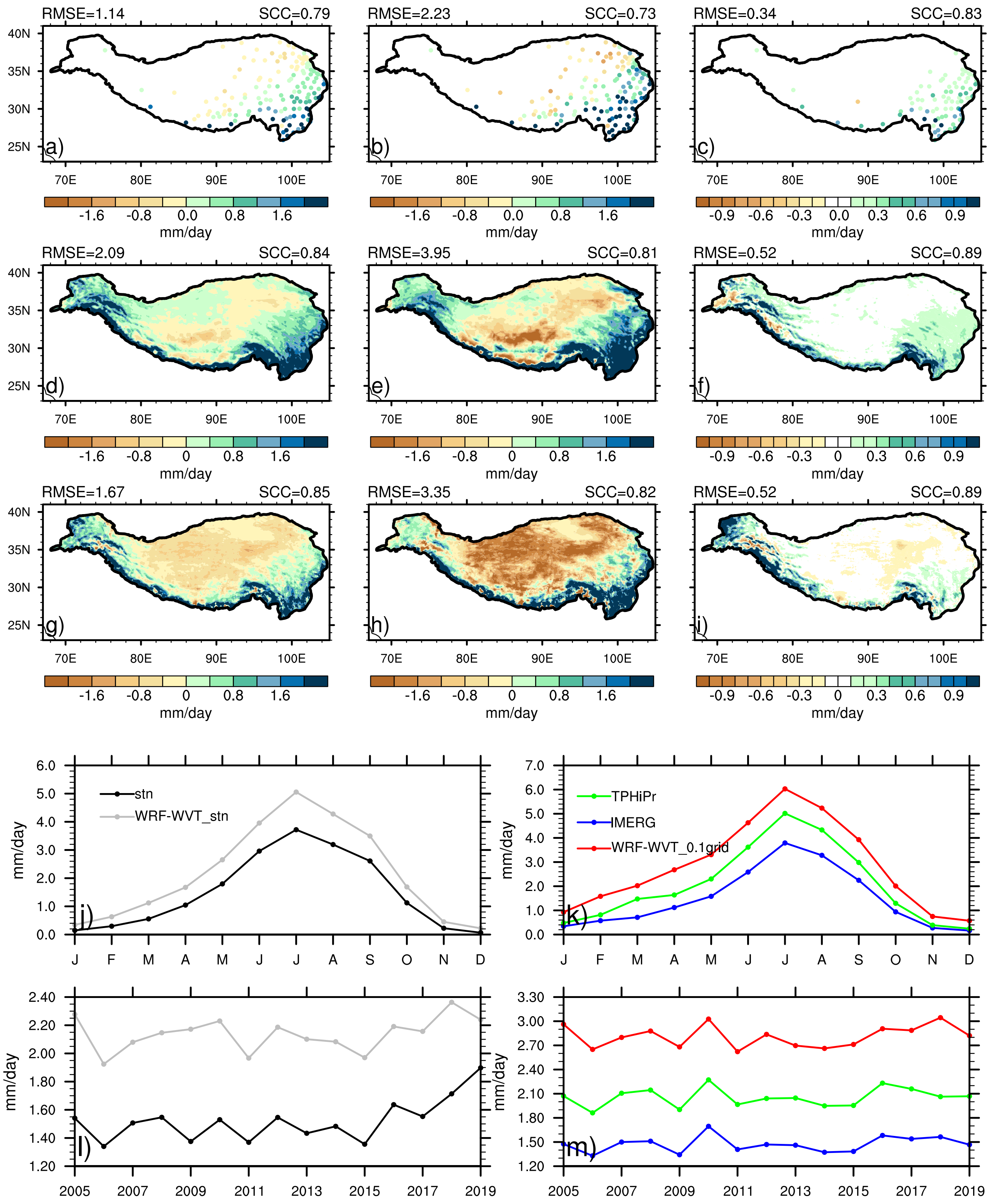

Figure 2. (a–c) Spatial pattern of biases in annual, summer, and winter mean precipitation compared to station observations, (d–f) IMERG data set, and (g–i) TPHiPr data set. Seasonal cycle and inter-annual variation of precipitation from in situ observation and WRF-WVT interpolated to station sites (j and l), as well as precipitation from gridded observations and WRF-WVT interpolated to 0.1° grid points (k and m).

10.1029/2023JD040230

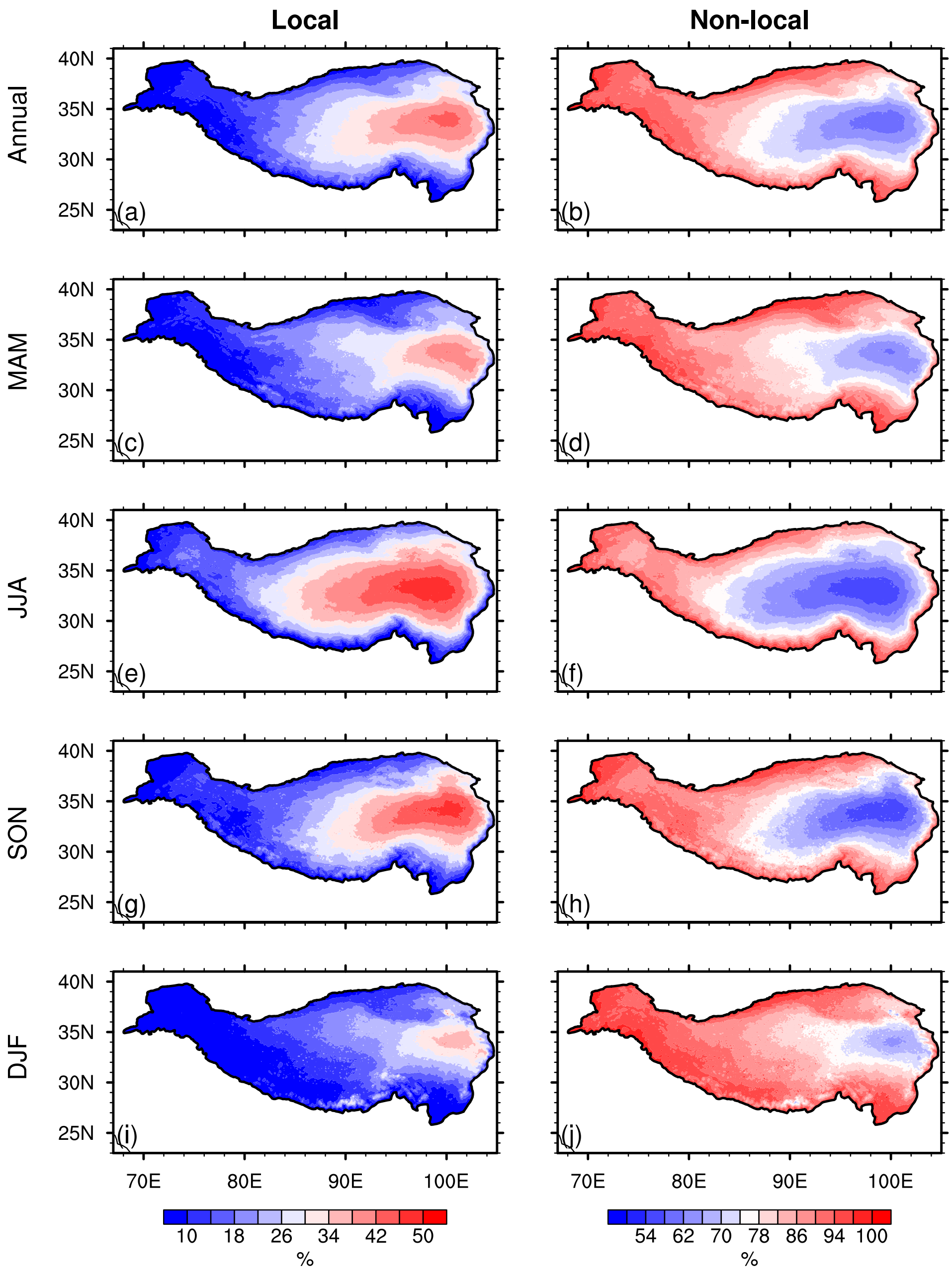

Figure 3. Spatial pattern of annual and seasonal mean fraction of traced precipitation to total precipitation from 2005 to 2019. The first column represents the fraction from local origin and the second column indicates the fraction from non-local origin.

investigating the factors that affect seasonal precipitation, both local and non-local factors are crucial. In light of the general knowledge of local evaporation and external water vapor advection above, the following analysis will focus on discussing their characteristics and their role in influencing the precipitation over the TP.

4.2. External Advected Water Vapor

4.2.1. Characteristics of External Water Vapor Transport

Figure 4 displays the longitude-pressure (latitude-pressure) profile of the zonal (meridional) WVTP combined with zonal (meridional) wind and enlarged vertical velocity, in order to firstly grasp a general understanding of how the water vapor enters and exits the TP. Two zonal WVTP centers are presented at the west of 80°E and east of 110°E (Figure 4a), respectively. Both WVTP centers are more obvious in summer and decline in winter,

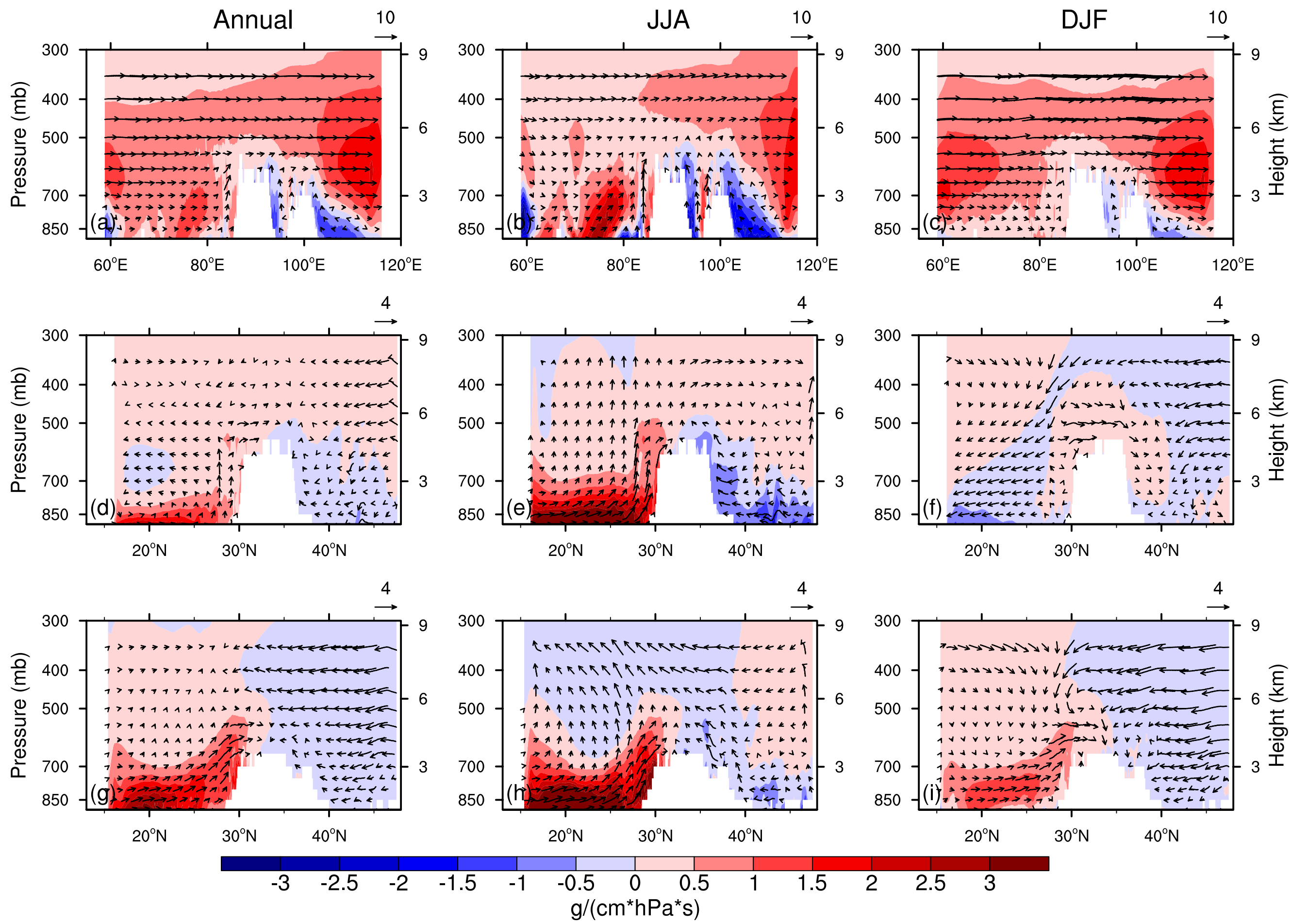

Figure 4. The first row shows the longitude-pressure profile of annual, summer and winter mean (a–c) zonal non-local water vapor transport (WVTP) (shadings) and wind field (vectors) encompassing zonal wind and vertical velocity (magnified by 100 times) averaged over 28°–35°N. The second row shows the latitude-pressure profile of the annual mean, summer, and winter mean (d–f) meridional WVTP (shadings) and wind field (vectors) encompassing meridional wind and vertical velocity (magnified by 100 times) averaged over 80°–95°E. The third row is similar to the second row, but averaged over 95°–102°E.

resulting in more (less) entrance of water vapor from the western boundary and export of water vapor from the eastern boundary in summer (winter). The prevailing westerly wind, which is stronger at the upper troposphere in winter, plays a role in facilitating the eastward large-scale WVTP; but the upward motion, which is stronger below 500 hPa, especially in summer, helps the water vapor climb up the TP, highlighting the importance of topography in modulating the WVTP. The meridional WVTP is more complex than zonal WVTP, since the altitude over the western TP is higher compared to the eastern TP. Therefore, the meridional WVTP is averaged over 80–95°E to represent the external WVTP toward western TP and over 95–102°E to represent that toward the eastern TP. The annual and seasonal mean meridional WVTP toward the western TP are generally weaker than those toward the eastern TP, decrease rapidly with height, and are constrained below 700 hPa and south of 30°N (Figures 4d and 4e); however, the meridional WVTP toward the eastern TP decreases more slowly with height and penetrates more upward to 500 hPa (Figure 4g) due to the existence of meridionally oriented valleys, which is more evident for annual and winter mean climatologies, allowing for more entrance of water vapor. The contrast of meridional WVTP toward western and eastern TP may partly explain the west–east gradient of precipitation. The wind field matches well with the meridional WVTP. Thus, the predominant entry of water vapor from the southern boundary is the meridional pathways at low- and mid-troposphere east of 95°E in summer.

Then, Figure 5 displays the inter-annual variations of several hydrological variables associated with the atmospheric water cycle over the TP from 2005 to 2019, in order to get more quantitative knowledge about the advected external water vapor, as well as its contribution to precipitation. Water vapor comes into (out of) the TP mainly via the western and southern (northern and eastern) boundary (denoted in Figure 1) with the annual

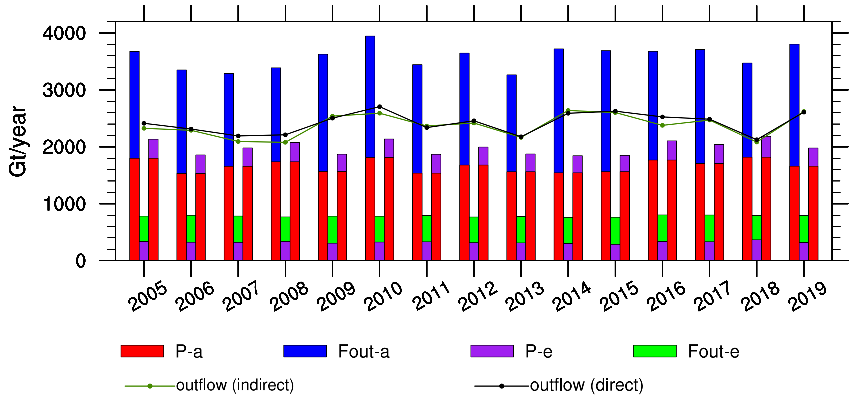

Figure 5. Annual amount of inflow of water vapor (the left bar in each year category), evaporation (the center bar in each year category), and total precipitation (the right bar in each year category). P-a and Fout-a denote precipitation contributed by external advected moisture and outflow of advected water vapor. P-e and Fout-e denote precipitation contributed by local evaporation and outflow of evaporative water vapor.

vertical integral of water vapor about 969.3 and 1,491.4 Gt (−236.4 and −1,061.6 Gt), leaving about 1,162.7 Gt water vapor over the TP involved in forming precipitation. Specifically, the outflow of water vapor is derived through two methods that (a) directly calculated with the method in Section 2.3 and (b) indirectly calculated based on the fact that outflow should be the sum of Fout-a (inflow minus P-a) and Fout-e (E minus P-e), respectively. It is clear that these two results resemble each other, and demonstrate very similar inter-annual variations. Therefore, a general sketch of the atmospheric hydrological cycle is obtained, and the rationality of calculating the inflow and outflow of water vapor with the subsection integral method is validated (since they are generally in coordination with the other simulated hydrological variables), laying foundation for establishing a robust relationship between external advected water vapor and precipitation next.

4.2.2. Role of External Advected Water Vapor in Influencing Precipitation

Establishing a connection between moisture transport and precipitation over the TP has gained a lot of attention recently. Table 1 lists the TCCs between the inflow, outflow, net income of water vapor, evaporation, and precipitation. The outflow of water vapor used hereinafter is calculated with the subsection integral method introduced in Section 2.3. It can be concluded that the inter-annual variation of precipitation is strongly linked to the net income of water vapor at both annual and seasonal scales, with the TCCs exceeding 0.80, especially in summer, indicating that the inter-annual variation of net income of water vapor dominates that of precipitation.

Using a threshold of one standard deviation, wet and dry years can be distinguished within the simulation period. The wet years consist of 2005, 2010 and 2018, while the dry years consist of 2006, 2014, and 2015. For external advected water vapor, based on Wei et al. (2016), the meridional (zonal) WVTP is represented as the multiplication of specific humidity q and meridional wind v (zonal wind u). The decomposition includes both the mean component and the transient eddy term. Then,

$$qv = (\overline{q} + \Delta q)(\overline{v} + \Delta v) = \overline{qv} + \overline{q}\Delta v + \overline{v}\Delta q + \Delta q \Delta v \quad (5)$$

$$qu = (\overline{q} + \Delta q)(\overline{u} + \Delta u) = \overline{qu} + \overline{q}\Delta u + \overline{u}\Delta q + \Delta q \Delta u \quad (6)$$

To illustrate the difference between meridional (zonal) WVTP and its mean state, the equations can be rewritten as:

$$qv - \overline{q}\,\overline{v} = \overline{q}\Delta v + \overline{v}\Delta q + \Delta q \Delta v \quad (7)$$

$$qu - \overline{q}\,\overline{u} = \overline{q}\Delta u + \overline{u}\Delta q + \Delta q \Delta u \quad (8)$$

Table 1
Temporal Correlation Coefficients (TCCs) Between Annual/Seasonal Inflow, Outflow, Net Income of Water Vapor (Net), Evaporation, and Precipitation During the Period 2005–2019

	Inflow	Outflow	Net	Evaporation
Annual	0.40	−0.03	0.89[a]	0.29
Spring	0.65[a]	−0.43	0.86[a]	0.39
Summer	0.59[a]	0.50[a]	0.97[a]	0.11
Autumn	0.20	0.17	0.83[a]	0.32
Winter	0.28	0.18	0.91[a]	0.25

[a]TCC has passed the 90% significance test.

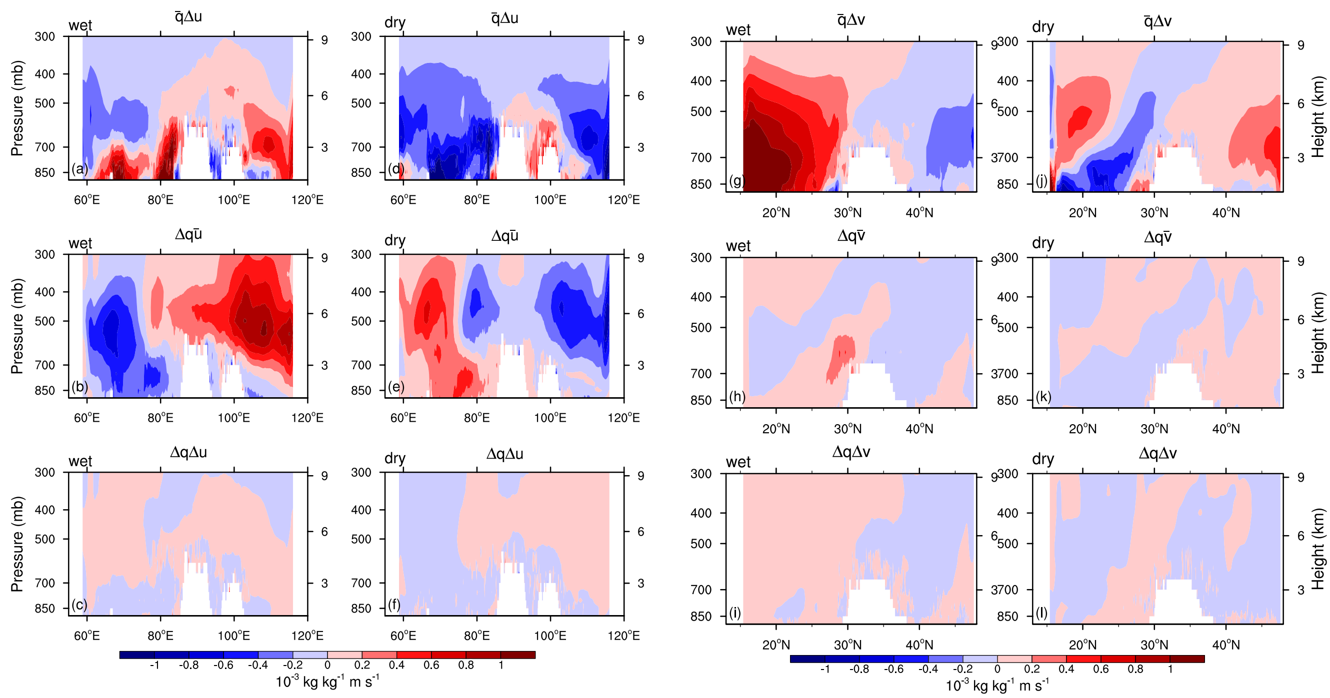

Figure 6. The first and second (third and fourth) column represent the longitude-pressure (latitude-pressure) cross section of moisture flux components for wet and dry years averaged over 28°–35°N (80°–102°E), respectively.

where ($\overline{q}\Delta v$; $\overline{q}\Delta u$), ($\overline{v}\Delta q$, $\overline{u}\Delta q$) and ($\Delta q\Delta v$, $\Delta q\Delta u$) represent differences caused by horizontal wind change, specific humidity change and a transient eddy term, respectively.

Figure 6 shows the zonal and meridional moisture flux components during wet/dry years. It can be discerned that the differences of external WVTP between wet and dry years can be attributed to the horizontal wind field alterations. Both the zonal westerly near 80°E and meridional southerly winds south of 30°N are substantially stronger during the wet years than dry years, indicating that the changes of horizontal wind have important influence on regulating the external WVTP toward the TP. Further investigation reveals that the precipitation differences during wet and dry periods are mainly contributed by the circulation changes-induced WVTP from the southern boundary, with the contribution of inflow reaching up to 89.0%, followed by water vapor escape from the eastern boundary (43.5%) (Table S1 in Supporting Information S1). The trumpet-shaped topography (TST) region is recognized as the probable key region for stronger WVTP into TP, excessive total column precipitable water originated from external sources regions and thus more precipitation during wet periods (Figure S3 in Supporting Information S1).

4.3. Local Recycling

4.3.1. Characteristics of PRR

Figure 7 displays the distributions of PRR, precipitation and evaporation versus elevation over the TP. For annual and summer mean PRR, general increases (decreases) with elevation of 2,000–4,750 m (4,750–6,000 m) are simulated; while for winter mean PRR, the vertical gradient of PRR and its maxima are smaller. The distributions of annual and seasonal mean vegetation fraction versus elevation are similar to those of precipitation. In contrast, the land-use category may play a major role in influencing the evaporation and further the precipitation recycling strength, with variations of grassland fraction with elevation in better agreement with evaporation and PRR, followed by open shrub. These can be interpreted in the way that, grasslands could enhance the precipitation contribution directly through evaporation (Y. Li et al., 2023). Since evaporation from grassland is probably driven by energy availability as proposed by Jansen et al. (2023), net radiation as indication of energy availability is compared between different land-use categories, and it turns out to be the possible drivers of stronger evaporation in grasslands as expected. In addition, considering the constraint of water vapor availability over the TP due to its towering terrain, the top layer soil moisture at 5 cm depth as indication of water availability is also investigated and is found to play a equally decisive role in triggering evaporation and favoring stronger precipitation recycling.

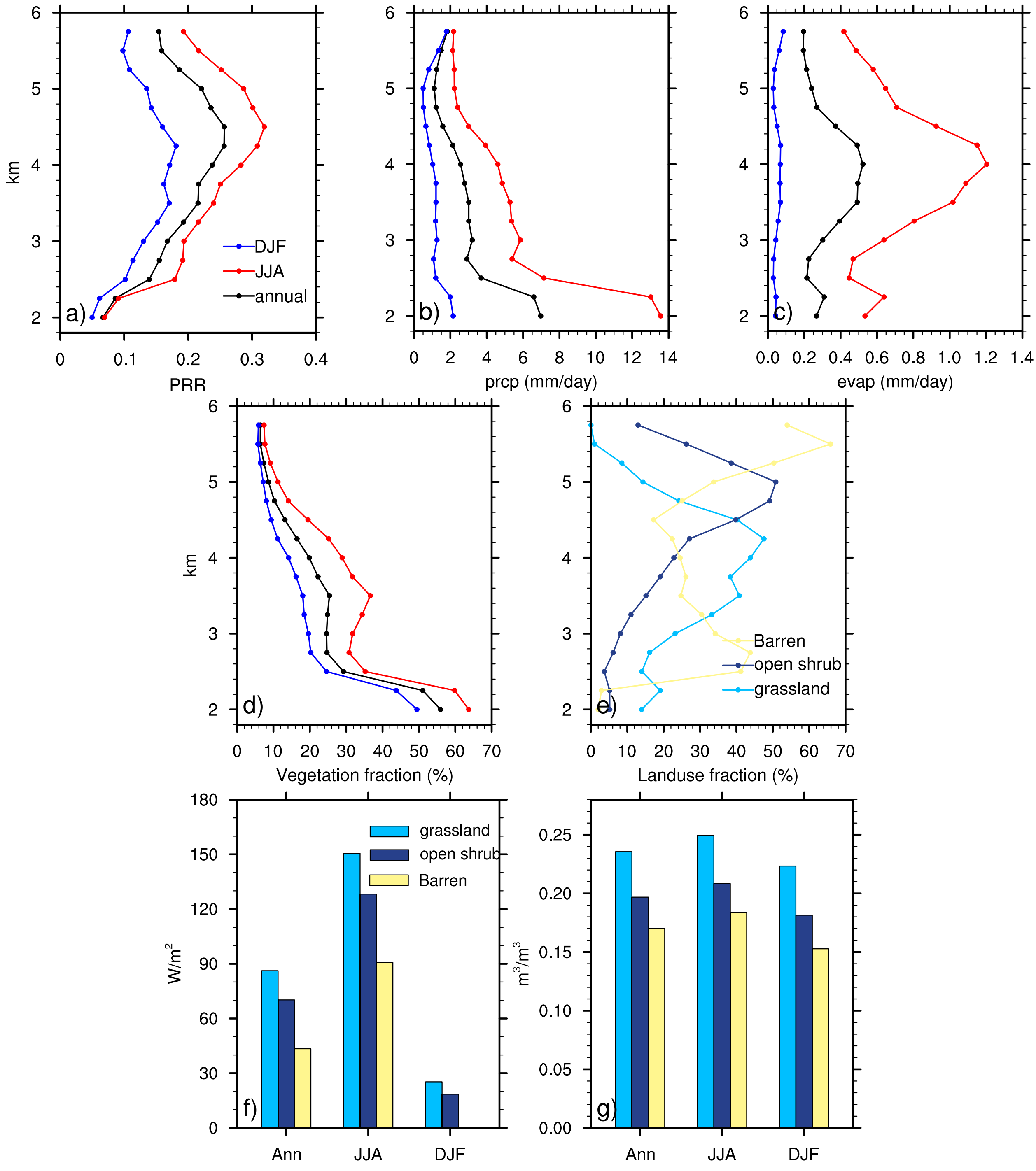

Figure 7. Annual, summer, and winter mean (a) Precipitation recycling ratio, (b) precipitation, (c) evaporation, (d) mean vegetation fraction, and (e) land-use category versus altitude with 250-m intervals over the Tibetan Plateau. Annual, summer, and winter mean (f) net radiation, and (g) soil moisture at 5 cm depth in grasslands, open shrubs and barren grounds.

In terms of the temporal characteristics of PRR and its linkage to precipitation, Figure 8 depicts the spatial pattern of PRR and precipitation peak timing at monthly timescale, as well as the variations of PRR and precipitation at inter-annual timescale. At intra-annual scale, over the eastern TP, the precipitation peak occurs in July, which is 1 month ahead of the PRR peak; over the northwestern TP, precipitation tends to peak in spring, which is much earlier than PRR. The postponed PRR peaks may be maintained by the soil moisture-precipitation feedback

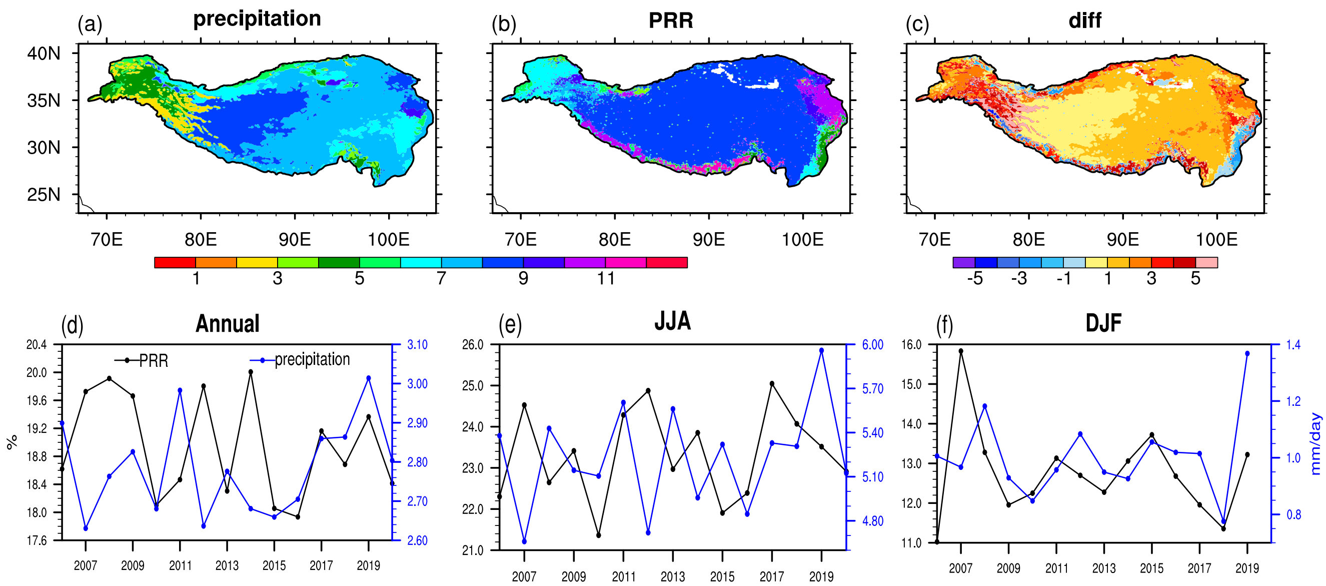

Figure 8. Spatial pattern of precipitation peak timing, Precipitation recycling ratio (PRR) peak timing, and their differences (represented by the deviation of PRR from precipitation) at monthly (a–c) scales. The inter-annual variation of annual (d), summer (e), and winter mean (f PRR (black lines)) and daily precipitation (blue lines). Note: If the deviation of PRR peak timing from precipitation is more than 6 months (less than −6 months), it is conversely considered that PRR changes are ahead of (behind) those of precipitation.

(Figure not shown). At inter-annual scale, there are more obviously asynchronous variations of precipitation and PRR, motivating more in-depth investigation into the factors that are critical in modulating the inter-annual variations of PRR.

4.3.2. Possible Reasons for the Inter-Annual Variation of PRR

Table 2 displays the TCCs between the inflow, outflow, net income of water vapor, evaporation and PRR. Unlike precipitation whose inter-annual variation is dominated by the net income of water vapor, the inter-annual variation of PRR is greatly influenced by the inflow and outflow of water vapor except for summer. There are significantly negative (positive) correlations between the inflow (outflow) of water vapor and PRR except for summer. This means that the more water vapor flows into (out of) the TP, the lower (higher) PRR is. However, for the inter-annual variation of summer mean PRR, local evaporation plays a leading role, with the significant TCC reaching 0.80.

As indicated in the above section, the inter-annual variations of inflow and outflow of water vapor are primarily dominated by the horizontal wind variations. Therefore, the 500 hPa wind velocity over the TP is used as an index to further explore the possible relationship between circulation strength and PRR. In addition to the dynamical factors, local heat fluxes (including latent and sensible heat fluxes), as important indication of the strength of local land surface-atmosphere interactions, may also play a role in PRR variations particularly in summer. In the following text, analysis will be centered around the modulation of both thermal and dynamical conditions to PRR variations.

Figure 9 displays the spatial pattern of TCCs between the inter-annual variation of horizontal wind velocity at 500 hPa and that of PRR at annual and seasonal scales. Dominant negative correlations are found between the inter-annual variations of low-level winds and those of PRRs in most regions of the TP, especially for spring and winter. This indicates that stronger winds not only facilitate the advection of more water vapor from external sources but also potentially drive a more substantial export of locally evaporated water vapor. Conversely, weaker winds may enhance the likelihood of locally evaporated water vapor re-precipitating within the TP and favor higher PRRs. Figure 10 shows the TCCs between seasonal PRR and dynamical factors

Table 2
Temporal Correlation Coefficients (TCCs) Between Inflow, Outflow, Net Income of Water Vapor (Net), Evaporation, Precipitation, and PRR

	Inflow	Outflow	Net	Evaporation	Precipitation
Annual	−0.84[a]	0.83[a]	−0.19	0.36	−0.09
Spring	−0.91[a]	0.90[a]	−0.46[a]	−0.18	−0.50[a]
Summer	−0.32	0.23	−0.10	0.80[a]	−0.14
Autumn	−0.70[a]	0.77[a]	−0.13	0.32	0.15
Winter	−0.69[a]	0.84[a]	0.21	−0.06	0.29

[a]TCC is significant at the 90% confidence level.

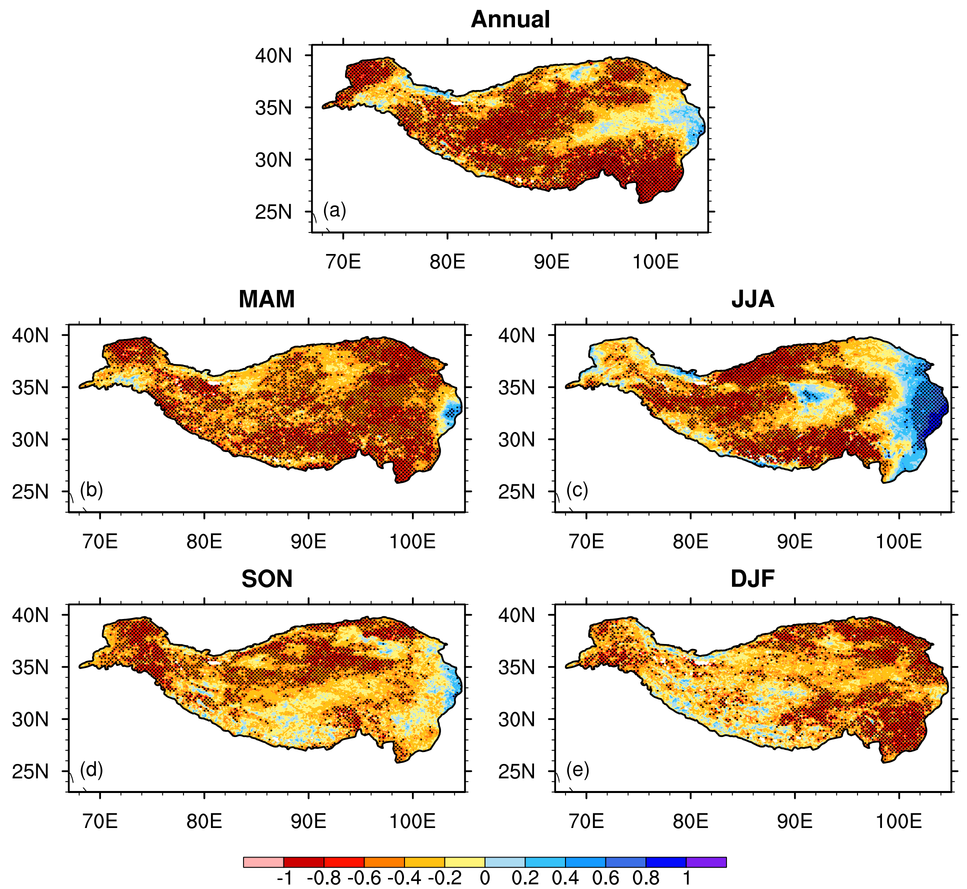

Figure 9. Spatial pattern of Temporal Correlation Coefficients (TCCs) between the inter-annual variation of (a) annual, (b) Spring, (c) Summer, (d) Fall, (e) Winter mean horizontal wind velocity at 500 hPa and that of the Precipitation recycling ratio. Dotted areas denote regions where TCCs are significant at the 90% confidence level.

(low-level wind velocity) as well as thermal factors (sensible and latent heat fluxes). Unlike spring and winter when the westerly wind prevails in the upper atmosphere and associated horizontal wind variations dominate those of PRR, it is noteworthy that latent and sensible heating could also make a great difference in summer and autumn, respectively. Positive correlation between summer latent heating and PRR, which is consistent with that between evaporation and PRR, emphasizes the role of summer evaporation. Enhanced sensible heating, as an indicator of decreased soil moisture (Cook et al., 2006), could probably result in less evaporated water vapor and lower PRR, which turns out to be the leading factor in autumn PRR variation. These imply that a combination of dynamical and thermal factors contributes greatly to the inter-annual variations of seasonal PRR.

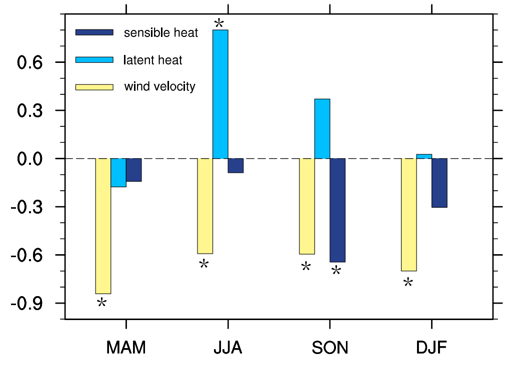

Figure 10. Temporal Correlation Coefficients (TCCs) between the inter-annual variation of Precipitation recycling ratio and 500 hPa horizontal wind velocity, latent heating, and sensible heating. In the figure, * denotes the TCC is significant at the 90% confidence level.

5. Discussion and Conclusions

In this study, we conducted an in-depth analysis of the contribution of local evaporation and remote WVTP to total precipitation over the TP. Employing WRF with WVTs to perform a high-resolution simulation spanning 15 years, we meticulously examined the spatiotemporal attributes of these moisture origins and their contributions to the inter-annual variation of precipitation.

The study discerns that water vapor entering through the southern boundary amounts to about 1,491.4 Gt/year, while that entering through the western boundary reaches up to 969.3 Gt/year. The northern and eastern boundary function as the main channels for water vapor export, with the estimation of

−236.4 Gt/year and −1,061.6 Gt/year, respectively. The WVTP-related precipitation consititutes the majority of total precipitation.

Exploring the relationship between WVTP and precipitation reveals a significantly positive correlation between the net income of water vapor and precipitation at inter-annual timescale, with high TCC exceeding 0.80. Further decomposition of moisture transport fluxes draws attention to the significant influence of changes in horizontal winds on water vapor inflow. Specifically, stronger (weaker) westerly and southerly winds play a crucial role in driving stronger (weaker) WVTP entering the TP, consequently impacting precipitation changes over the region. Particularly, circulation changes-induced WVTP from the southern boundary contributes the most (~89.0%) to precipitation variations, especially over the TST region.

The study also reveals distinct variations in the PRR with respect to elevation over the TP. PRR peaks around 4,750 m in summer but at slightly lower altitudes during winter. Interestingly, the distribution of PRR concerning elevation aligns more with the fraction of grasslands which, with more energy and water availability, may influence PRR by directly triggering stronger evaporation. From the perspective of temporal variations, there are asynchronous changes in PRR and precipitation at both intra-annual and inter-annual scales. While the previously reported soil moisture-precipitation feedback is identified, no significant linkage is observed between PRR and precipitation at inter-annual timescale.

The inter-annual variation of PRR is found to be strongly correlated with the variation of external advected water vapor and associated wind strength at 500 hPa, especially during the colder season. However, thermal factors, encompassing sensible and latent heating, demonstrate equal importance in modulating the inter-annual variation of summer and autumn mean PRR. This emphasizes that a combination of dynamical and thermal factors involved in land surface–atmosphere interactions profoundly impacts precipitation recycling processes across various spatial and temporal scales, warranting further research.

Finally, it is worth mentioning that, our findings are heavily dependent on the model representations by WRF-WVT which is a comparatively reliable and precise method for tracking atmospheric moisture pathways, getting rid of the shortcomings of most analytical models. While WRF-WVT successfully reproduces the pattern of surface variables and large-scale dynamic and thermodynamic features (Figures S4–S9 and Table S2 in Supporting Information S1), annual and seasonal precipitation is overestimated (underestimated) mainly over the southeastern (central) TP. Likewise, the model tends to overestimate (underestimate) the evaporation, as indicated by the slightly overestimated (underestimated) latent heat fluxes (Figure S9 in Supporting Information S1), and evaporation-associated precipitation there, while its impact on PRR is uncertain without reliable observation-based estimations (e.g., stable isotopes) (Hu & Dominguez, 2019). Besides, the PBL parameterization could also affect precipitation simulation through land-atmosphere interactions (Dominguez et al., 2016). Therefore, future model improvements in enabling the application of WVTs to other physical parameterizations within WRF and enhancing observation monitoring to obtain moisture origin features are supposed to better constrain models and diminish uncertainties in the PRR estimation. Nevertheless, here in this study, our focus is the relative importance of local evaporated and external advected moisture to precipitation's inter-annual variation. Based on generally well-captured inter-annual variations of dynamic and thermodynamic variables (Table S2 in Supporting Information S1), the primary relationship between precipitation and its likely governing factors are supposed to have certain credibility. These findings are expected to provide some experience for future in-depth investigations in this field.

Data Availability Statement

The WRF model version 4.3.3, used to generate the simulation in this study, is available from Skamarock et al. (2019). The WVTs implementated in the WRF model is accessible from Insua-Costa and Miguez-Macho (2018). The ERA5 data set can be obtained from Hersbach et al. (2020). The station observations can be accessed at: http://data.cma.cn/en. The IMERG data set can be downloaded from Huffman et al. (2020). The TPHiPr data set is available at Jiang et al. (2023). The data and codes related to statistical analysis are accessible from Ma et al. (2023c).

Acknowledgments

The research is supported by the Second Tibetan Plateau Scientific Expedition and Research Program (STEP, Grant 2019QZKK0206), the National Key Research and Development Program of China (2018YFA0606003), the National Natural Science Foundation of China (41875124), the Swedish Foundation for International Cooperation in Research and Higher Education (CH2020-8767) and Swedish Research Council (VR: 2019-03954). Chen and Ou are supported by the Strategic Research Area "ModElling the Regional and Global Earth system," MERGE, funded by the Swedish government.

References

An, W., Hou, S., Zhang, Q., Zhang, W., Wu, S., Xu, H., et al. (2017). Enhanced recent local moisture recycling on the northwestern Tibetan Plateau deduced from ice core deuterium excess records. *Journal of Geophysical Research: Atmospheres*, *122*(23), 12541–12556. https://doi.org/10.1002/2017jd027235

Bosilovich, M. G. (2002). On the vertical distribution of local and remote sources of water for precipitation. *Meteorology and Atmospheric Physics*, *80*(1–4), 31–41. https://doi.org/10.1007/s007030200012

Brubaker, K. L., Dirmeyer, P. A., Sudradjat, A., Levy, B. S., & Bernal, F. (2001). A 36-yr climatological description of the evaporative sources of warm-season precipitation in the Mississippi River basin. *Journal of Hydrometeorology*, *2*(6), 537–557. https://doi.org/10.1175/1525-7541(2001)002<0537:aycdot>2.0.co;2

Brubaker, K. L., Entekhabi, D., & Eagleson, P. S. (1993). Estimation of continental precipitation recycling. *Journal of Climate*, *6*(6), 1077–1089. https://doi.org/10.1175/1520-0442(1993)006<1077:eocpr>2.0.co;2

Burde, G., & Zangvil, A. (2001a). The estimation of regional precipitation recycling. Part I: Review of recycling models. *Journal of Climate*, *14*(12), 2497–2508. https://doi.org/10.1175/1520-0442(2001)014<2497:TEORPR>2.0.CO;2

Burde, G., & Zangvil, A. (2001b). The estimation of regional precipitation recycling. Part II: A new recycling model. *Journal of Climate*, *14*(12), 2509–2527. https://doi.org/10.1175/1520-0442(2001)014<2509:TEORPR>2.0.CO;2

Buytaert, W., Vuille, M., Dewulf, A., Urrutia, R., Karmalkar, A., & Célleri, R. (2010). Uncertainties in climate change projections and regional downscaling in the tropical Andes: Implications for water resources management. *Hydrology and Earth System Sciences*, *14*(7), 1247–1258. https://doi.org/10.5194/hess-14-1247-2010

Cai, Z., & Tian, L. (2016). Atmospheric controls on seasonal and interannual variations in the precipitation isotope in the East Asian monsoon region. *Journal of Climate*, *29*(4), 1339–1352. https://doi.org/10.1175/jcli-d-15-0363.1

Cannon, F., Carvalho, L. M. V., Jones, C., Hoell, A., Norris, J., Kiladis, G. N., & Tahir, A. A. (2017). The influence of tropical forcing on extreme winter precipitation in the Western Himalaya. *Climate Dynamics*, *48*(3–4), 1213–1232. https://doi.org/10.1007/s00382-016-3137-0

Chao, N., Wang, Z., Hwang, C., Jin, T., & Cheng, Y.-S. (2017). Decline of Geladandong glacier elevation in Yangtze River's source region: Detection by ICESat and assessment by hydroclimatic data. *Remote Sensing*, *9*(1), 75. https://doi.org/10.3390/rs9010075

Chen, B., Xu, X.-D., Yang, S., & Zhang, W. (2012). On the origin and destination of atmospheric moisture and air mass over the Tibetan Plateau. *Theoretical and Applied Climatology*, *110*(3), 423–435. https://doi.org/10.1007/s00704-012-0641-y

Chen, B., Zhang, W., Yang, S., & Xu, X. (2019). Identifying and contrasting the sources of the water vapor reaching the subregions of the Tibetan Plateau during the wet season. *Climate Dynamics*, *53*(11), 6891–6907. https://doi.org/10.1007/s00382-019-04963-2

Chen, F., & Dudhia, J. (2001). Coupling an advanced land surface–hydrology model with the Penn State–NCAR MM5 modeling system. Part I: Model implementation and sensitivity. *Monthly Weather Review*, *129*(4), 569–585. https://doi.org/10.1175/1520-0493(2001)129<0569:caalsh>2.0.co;2

Ciric, D., Nieto, R., Losada, L., Drumond, A., & Gimeno, L. (2018). The Mediterranean moisture contribution to climatological and extreme monthly continental precipitation. *Water*, *10*(4), 519. https://doi.org/10.3390/w10040519

Cook, B. I., Bonan, G. B., & Levis, S. (2006). Soil moisture feedbacks to precipitation in Southern Africa. *Journal of Climate*, *19*(17), 4198–4206. https://doi.org/10.1175/jcli3856.1

Cuo, L., & Zhang, Y. (2017). Spatial patterns of wet season precipitation vertical gradients on the Tibetan Plateau and the surroundings. *Scientific Reports*, *7*(1), 5057. https://doi.org/10.1038/s41598-017-05345-6

Curio, J., Maussion, F., & Scherer, D. (2015). A 12-year high-resolution climatology of atmospheric water transport over the Tibetan Plateau. *Earth System Dynamics*, *6*(1), 109–124. https://doi.org/10.5194/esd-6-109-2015

Curio, J., & Scherer, D. (2016). Seasonality and spatial variability of dynamic precipitation controls on the Tibetan Plateau. *Earth System Dynamics*, *7*(3), 767–782. https://doi.org/10.5194/esd-7-767-2016

Dirmeyer, P. A., & Brubaker, K. L. (2006). Evidence for trends in the Northern Hemisphere water cycle. *Geophysical Research Letters*, *33*(14), 83–95. https://doi.org/10.1029/2006gl026359

Dominguez, F., Eiras-Barca, J., Yang, Z., Bock, D., Nieto, R., & Gimeno, L. (2022). Amazonian moisture recycling revisited using WRF with water vapor tracers. *Journal of Geophysical Research: Atmospheres*, *127*(4), e2021JD035259. https://doi.org/10.1029/2021jd035259

Dominguez, F., Kumar, P., Liang, X.-Z., & Ting, M. (2006). Impact of atmospheric moisture storage on precipitation recycling. *Journal of Climate*, *19*(8), 1513–1530. https://doi.org/10.1175/JCLI3691.1

Dominguez, F., Miguez-Macho, G., & Hu, H. (2016). WRF with water vapor tracers: A study of moisture sources for the North American monsoon. *Journal of Hydrometeorology*, *17*(7), 1915–1927. https://doi.org/10.1175/jhm-d-15-0221.1

Dong, W., Lin, Y., Wright, J. S., Ming, Y., Xie, Y., Wang, B., et al. (2016). Summer rainfall over the southwestern Tibetan Plateau controlled by deep convection over the Indian subcontinent. *Nature Communications*, *7*(1), 10925. https://doi.org/10.1038/ncomms10925

Eiras-Barca, J., Dominguez, F., Hu, H., Garaboa-Paz, D., & Miguez-Macho, G. (2017). Evaluation of the moisture sources in two extreme landfalling atmospheric river events using an Eulerian WRF tracers tool. *Earth System Dynamics*, *8*(4), 1247–1261. https://doi.org/10.5194/esd-8-1247-2017

Eltahir, E. A., & Bras, R. L. (1994). Precipitation recycling in the Amazon Basin. *Quarterly Journal of the Royal Meteorological Society*, *120*(518), 861–880. https://doi.org/10.1002/qj.49712051806

Eltahir, E. A., & Bras, R. L. (1996). Precipitation recycling. *Reviews of Geophysics*, *34*(3), 367–378. https://doi.org/10.1029/96RG01927

Feng, L., & Zhou, T. (2012). Water vapor transport for summer precipitation over the Tibetan Plateau: Multidata set analysis. *Journal of Geophysical Research*, *117*(D20), D20114. https://doi.org/10.1029/2011jd017012

Gao, J., Yao, T., Masson-Delmotte, V., Steen-Larsen, H. C., & Wang, W. (2019). Collapsing glaciers threaten Asia's water supplies. *Nature*, *565*(7737), 19–21. https://doi.org/10.1038/d41586-018-07838-4

Gao, Y., Chen, F., Miguez-Macho, G., & Li, X. (2020). Understanding precipitation recycling over the Tibetan Plateau using tracer analysis with WRF. *Climate Dynamics*, *55*(9–10), 2921–2937. https://doi.org/10.1007/s00382-020-05426-9

Gimeno, L., Drumond, A., Nieto, R., Trigo, R. M., & Stohl, A. (2010). On the origin of continental precipitation. *Geophysical Research Letters*, *37*(13), L13804. https://doi.org/10.1029/2010gl043712

Gimeno, L., Stohl, A., Trigo, R. M., Dominguez, F., Yoshimura, K., Yu, L., et al. (2012). Oceanic and terrestrial sources of continental precipitation. *Reviews of Geophysics*, *50*(4), RG4003. https://doi.org/10.1029/2012rg000389

Gimeno Presa, L., Vázquez, M., Eiras Barca, J., Sorí, R., Stojanovic, M., Algarra, I., et al. (2020). Recent progress on the sources of continental precipitation as revealed by moisture transport analysis. https://doi.org/10.1016/j.earscirev.2019.103070

Guo, L., Klingaman, N. P., Demory, M.-E., Vidale, P. L., Turner, A. G., & Stephan, C. C. (2018). The contributions of local and remote atmospheric moisture fluxes to East Asian precipitation and its variability. *Climate Dynamics*, *51*(11–12), 4139–4156. https://doi.org/10.1007/s00382-017-4064-4

Guo, X., Tian, L., Wen, R., Yu, W., & Qu, D. (2017). Controls of precipitation δ^{18}O on the NORTHWESTERN Tibetan plateau: A case study at Ngari station. *Atmospheric Research*, *189*, 141–151. https://doi.org/10.1016/j.atmosres.2017.02.004

Hersbach, H., Bell, B., Berrisford, P., Hirahara, S., Horányi, A., Muñoz-Sabater, J., et al. (2020). The ERA5 global reanalysis [Dataset]. *Quarterly Journal of the Royal Meteorological Society*, *146*(730), 1999–2049. https://doi.org/10.1002/qj.3803

Hong, S.-Y., & Lim, J.-O. J. (2006). The WRF single-moment 6-class microphysics scheme (WSM6). *Asia-Pacific Journal of Atmospheric Sciences*, *42*(2), 129–151.

Hong, S.-Y., Noh, Y., & Dudhia, J. (2006). A new vertical diffusion package with an explicit treatment of entrainment processes. *Monthly Weather Review*, *134*(9), 2318–2341. https://doi.org/10.1175/mwr3199.1

Hu, H., & Dominguez, F. (2019). Understanding the role of tropical moisture in atmospheric rivers. *Journal of Geophysical Research: Atmospheres*, *124*(24), 13826–13842. https://doi.org/10.1029/2019jd030867

Huang, W., Qiu, T., Yang, Z., Lin, D., Wright, J. S., Wang, B., & He, X. (2018). On the formation mechanism for wintertime extreme precipitation events over the Southeastern Tibetan Plateau. *Journal of Geophysical Research: Atmospheres*, *123*(22), 12692–12714. https://doi.org/10.1029/2018jd028921

Huffman, G. J., Bolvin, D. T., Braithwaite, D., Hsu, K.-L., Joyce, R. J., Kidd, C., et al. (2020). Integrated multi-satellite Retrievals for the Global Precipitation Measurement (GPM) mission (IMERG). [Dataset]. *Springer International Publishing*, 343–353. https://doi.org/10.1007/978-3-030-24568-9_19

Iacono, M. J., Delamere, J. S., Mlawer, E. J., Shephard, M. W., Clough, S. A., & Collins, W. D. (2008). Radiative forcing by long-lived greenhouse gases: Calculations with the AER radiative transfer models. *Journal of Geophysical Research*, *113*(D13), D13103. https://doi.org/10.1029/2008jd009944

Immerzeel, W. W., Van Beek, L. P., & Bierkens, M. F. (2010). Climate change will affect the Asian water towers. *Science*, *328*(5984), 1382–1385. https://doi.org/10.1126/science.1183188

Insua-Costa, D., & Miguez-Macho, G. (2018). A new moisture tagging capability in the weather research and forecasting model: Formulation, validation and application to the 2014 great lake-effect Snowstorm [Software]. *Earth System Dynamics*, *9*(1), 167–185. https://doi.org/10.5194/esd-9-167-2018

James, P., Stohl, A., Spichtinger, N., Eckhardt, S., & Forster, C. (2004). Climatological aspects of the extreme European rainfall of August 2002 and a trajectory method for estimating the associated evaporative source regions. *Natural Hazards and Earth System Sciences*, *4*(5/6), 733–746. https://doi.org/10.5194/nhess-4-733-2004

Jansen, F. A., Jongen, H. J., Jacobs, C. M. J., Bosveld, F. C., Buzacott, A. J. V., Heusinkveld, B. G., et al. (2023). Land cover control on the drivers of evaporation and sensible heat fluxes: An observation-based synthesis for The Netherlands. *Water Resources Research*, *59*(11), e2022WR034361. https://doi.org/10.1029/2022wr034361

Jia, P., Zhuang, D., & Wang, Y. (2017). Impacts of temperature and precipitation on the spatiotemporal distribution of water resources in Chinese mega cities: The case of Beijing. *Journal of Water and Climate Change*, *8*(4), 593–612. https://doi.org/10.2166/wcc.2017.038

Jiang, Y., Yang, K., Qi, Y., Zhou, X., He, J., Lu, H., et al. (2023). TPHiPr: A long-term (1979–2020) high-accuracy precipitation dataset (1/30°, daily) for the third Pole region based on high-resolution atmospheric modeling and dense observations [Dataset]. *Earth System Science Data*, *15*(2), 621–638. https://doi.org/10.5194/essd-15-621-2023

Juan, G., Zongxing, L., Qi, F., Baijuan, Z., Jian, X., Wende, G., et al. (2022). Water resources significance of moisture recycling in the transition zone between Tibetan Plateau and arid region by stable isotope tracing. *Journal of Hydrology*, *605*, 127350. https://doi.org/10.1016/j.jhydrol.2021.127350

Knoche, H. R., & Kunstmann, H. (2013). Tracking atmospheric water pathways by direct evaporation tagging: A case study for West Africa. *Journal of Geophysical Research: Atmospheres*, *118*(22), 12345–12358. https://doi.org/10.1002/2013jd019976

Koster, R., Jouzel, J., Suozzo, R., Russell, G., Broecker, W., Rind, D., & Eagleson, P. (1986). Global sources of local precipitation as determined by the NASA/GISS GCM. *Geophysical Research Letters*, *13*(2), 121–124. https://doi.org/10.1029/gl013i002p00121

Li, X., Wu, P., Ding, Y., Liu, Y., & Li, Q. (2022). Spatial-temporal variation of precipitation recycling over the Tibetan Plateau under climate warming. *Atmospheric Research*, *280*, 106431. https://doi.org/10.1016/j.atmosres.2022.106431

Li, Y., Su, F., Tang, Q., Gao, H., Yan, D., Peng, H., & Xiao, S. (2022). Contributions of moisture sources to precipitation in the major drainage basins in the Tibetan Plateau. *Science China Earth Sciences*, *65*(6), 1088–1103. https://doi.org/10.1007/s11430-021-9890-6

Li, Y., Xu, R., Yang, K., Liu, Y., Wang, S., Zhou, S., et al. (2023). Contribution of Tibetan Plateau ecosystems to local and remote precipitation through moisture recycling. *Global Change Biology*, *29*(3), 702–718. https://doi.org/10.1111/gcb.16495

Li, Z., Gong, X., Wei, X., & Yang, j. (2019). Precipitation trends and alteration in Wei river basin: Implication for water resources management in the transitional zone between plain and loess Plateau, China. *Water*, *11*(11), 2407. https://doi.org/10.3390/w11112407

Liu, W., Xu, Z., Li, F., Zhang, L., Zhao, J., & Yang, H. (2015). Impacts of climate change on hydrological processes in the Tibetan Plateau: A case study in the lhasa river Basin. *Stochastic Environmental Research and Risk Assessment*, *29*(7), 1809–1822. https://doi.org/10.1007/s00477-015-1066-9

Liu, Z., Yao, Z., Wang, R., & Yu, G. (2020). Estimation of the Qinghai-Tibetan Plateau runoff and its contribution to large Asian rivers. *Science of the Total Environment*, *749*, 141570. https://doi.org/10.1016/j.scitotenv.2020.141570

Ma, M., Hui, P., Liu, D., Zhou, P., & Tang, J. (2021). Convection-permitting regional climate simulations over Tibetan plateau: Re-initialization versus spectral nudging. *Climate Dynamics*, *58*(5–6), 1719–1735. https://doi.org/10.1007/s00382-021-05988-2

Ma, M., Ou, T., Liu, D., Wang, S., Fang, J., & Tang, J. (2023a). Summer regional climate simulations over Tibetan Plateau: From gray zone to convection permitting scale. *Climate Dynamics*, *60*(1–2), 301–322. https://doi.org/10.1007/s00382-022-06314-0

Ma, M., Tang, J., Ou, T., & Chen, D. (2023c). Contribution of recycled and external advected moisture to precipitation and its inter-annual variation over the Tibetan Plateau [Dataset]. *Zenodo*. https://doi.org/10.5281/zenodo.8420441

Ma, M., Tang, J., Ou, T., & Zhou, P. (2023b). High-resolution climate projection over the Tibetan Plateau using WRF forced by bias-corrected CESM. *Atmospheric Research*, *286*, 106670. https://doi.org/10.1016/j.atmosres.2023.106670

Ma, Y., Lu, M., Chen, H., Pan, M., & Hong, Y. (2018). Atmospheric moisture transport versus precipitation across the Tibetan Plateau: A mini-review and current challenges. *Atmospheric Research*, *209*, 50–58. https://doi.org/10.1016/j.atmosres.2018.03.015

Maussion, F., Scherer, D., Mölg, T., Collier, E., Curio, J., & Finkelnburg, R. (2014). Precipitation seasonality and variability over the Tibetan Plateau as resolved by the high Asia reanalysis. *Journal of Climate*, *27*(5), 1910–1927. https://doi.org/10.1175/jcli-d-13-00282.1

Numaguti, A. (1999). Origin and recycling processes of precipitating water over the Eurasian continent: Experiments using an atmospheric general circulation model. *Journal of Geophysical Research*, *104*(D2), 1957–1972. https://doi.org/10.1029/1998jd200026

Ou, T., Chen, D., Tang, J., Lin, C., Wang, X., Kukulies, J., & Lai, H.-W. (2023). Wet bias of summer precipitation in the northwestern Tibetan Plateau in ERA5 is linked to overestimated lower-level southerly wind over the Plateau. *Climate Dynamics*, *61*(5–6), 2139–2153. https://doi.org/10.1007/s00382-023-06672-3

Pan, C., Zhu, B., Gao, J., Kang, H., & Zhu, T. (2019). Quantitative identification of moisture sources over the Tibetan Plateau and the relationship between thermal forcing and moisture transport. *Climate Dynamics*, *52*(1–2), 181–196. https://doi.org/10.1007/s00382-018-4130-6

Qu, B., Zhang, Y., Kang, S., & Sillanpää, M. (2019). Water quality in the Tibetan Plateau: Major ions and trace elements in rivers of the "water tower of Asia". *Science of the Total Environment*, *649*, 571–581. https://doi.org/10.1016/j.scitotenv.2018.08.316

Singh, H. A., Bitz, C. M., Nusbaumer, J., & Noone, D. C. (2016). A mathematical framework for analysis of water tracers: Part 1: Development of theory and application to the preindustrial mean state. *Journal of Advances in Modeling Earth Systems*, *8*(2), 991–1013. https://doi.org/10.1002/2016ms000649

Skamarock, W. C., Klemp, J. B., Dudhia, J., Gill, D. O., Liu, Z., Berner, J., et al. (2019). A description of the advanced research WRF model version 4 [Software]. *National Center for Atmospheric Research*, *145*, 550. https://doi.org/10.5065/1dfh-6p97

Sodemann, H., Wernli, H., & Schwierz, C. (2009). Sources of water vapour contributing to the Elbe flood in August 2002—A tagging study in a mesoscale model. *Quarterly Journal of the Royal Meteorological Society*, *135*(638), 205–223. https://doi.org/10.1002/qj.374

Stohl, A. (1998). Computation, accuracy and applications of trajectories—A review and bibliography. *Atmospheric Environment*, *32*(6), 947–966. https://doi.org/10.1016/S1352-2310(97)00457-3

Stohl, A., & James, P. (2004). A Lagrangian analysis of the atmospheric branch of the global water cycle. Part I: Method description, validation, and demonstration for the August 2002 flooding in central Europe. *Journal of Hydrometeorology*, *5*(4), 656–678. https://doi.org/10.1175/1525-7541(2004)005<0656:alaota>2.0.co;2

Stohl, A., & James, P. (2005). A Lagrangian analysis of the atmospheric branch of the global water cycle. Part 2: Earth's river catchments, ocean basins, and moisture transports between them. *Journal of Hydrometeorology*, *6*, 961–984. https://doi.org/10.1175/JHM470.1

Tan, J., Petersen, W. A., Kirstetter, P. E., & Tian, Y. (2017). Performance of IMERG as a function of spatiotemporal scale. *Journal of Hydrometeorology*, *18*(2), 307–319. https://doi.org/10.1175/JHM-D-16-0174.1

Trenberth, K. E. (1999). Atmospheric moisture recycling: Role of advection and local evaporation. *Journal of Climate*, *12*(5), 1368–1381. https://doi.org/10.1175/1520-0442(1999)012<1368:amrroa>2.0.co;2

Wang, Z., Duan, A., Yang, S., & Ullah, K. (2017). Atmospheric moisture budget and its regulation on the variability of summer precipitation over the Tibetan Plateau. *Journal of Geophysical Research: Atmospheres*, *122*(2), 614–630. https://doi.org/10.1002/2016jd025515

Wei, J., Su, H., & Yang, Z.-L. (2016). Impact of moisture flux convergence and soil moisture on precipitation: A case study for the Southern United States with implications for the globe. *Climate Dynamics*, *46*(1–2), 467–481. https://doi.org/10.1007/s00382-015-2593-2

Werner, M., Heimann, M., & Hoffmann, G. (2001). Isotopic composition and origin of polar precipitation in present and glacial climate simulations. *Tellus B: Chemical and Physical Meteorology*, *53*(1), 53. https://doi.org/10.3402/tellusb.v53i1.16539

Xu, X., Lu, C., Shi, X., & Gao, S. (2008). World water tower: An atmospheric perspective. *Geophysical Research Letters*, *35*(20), L20815. https://doi.org/10.1029/2008gl035867

Xu, Y., & Gao, Y. (2019). Quantification of evaporative sources of precipitation and its changes in the Southeastern Tibetan Plateau and middle Yangtze River basin. *Atmosphere*, *10*(8), 428. https://doi.org/10.3390/atmos10080428

Yan, H., Huang, J., He, Y., Liu, Y., Wang, T., & Li, J. (2020). Atmospheric water vapor budget and its long-term trend over the Tibetan plateau. *Journal of Geophysical Research: Atmospheres*, *125*(23), e2020JD033297. https://doi.org/10.1029/2020jd033297

Yao, T., Bolch, T., Chen, D., Gao, J., Immerzeel, W., Piao, S., et al. (2022). The imbalance of the Asian water tower. *Nature Reviews Earth and Environment*, *3*(10), 618–632. https://doi.org/10.1038/s43017-022-00299-4

Yao, T., Masson-Delmotte, V., Gao, J., Yu, W., Yang, X., Risi, C., et al. (2013). A review of climatic controls on $\delta^{18}O$ in precipitation over the Tibetan Plateau: Observations and simulations. *Reviews of Geophysics*, *51*(4), 525–548. https://doi.org/10.1002/rog.20023

Yao, T.-D., Qin, D.-H., Shen, Y.-P., Zhao, L., Wang, N., & Lu, A. (2013). Cryospheric changes and their impacts on regional water cycle and ecological conditions in the Qinghai-Tibetan Plateau. *Chinese Journal of Nature*, *35*(3), 179–186.

Zhang, C., Tang, Q., & Chen, D. (2017). Recent changes in the moisture source of precipitation over the Tibetan Plateau. *Journal of Climate*, *30*(5), 1807–1819. https://doi.org/10.1175/jcli-d-15-0842.1

Zhang, C., Tang, Q., Chen, D., Van Der Ent, R. J., Liu, X., Li, W., & Haile, G. G. (2019). Moisture source changes contributed to different precipitation changes over the northern and southern Tibetan Plateau. *Journal of Hydrometeorology*, *20*(2), 217–229. https://doi.org/10.1175/jhm-d-18-0094.1

Zhang, L., Su, F., Yang, D., Hao, Z., & Tong, K. (2013). Discharge regime and simulation for the upstream of major rivers over Tibetan Plateau. *Journal of Geophysical Research: Atmospheres*, *118*(15), 8500–8518. https://doi.org/10.1002/jgrd.50665

Zhao, Y., & Zhou, T. (2021). Interannual variability of precipitation recycle ratio over the Tibetan Plateau. *Journal of Geophysical Research: Atmospheres*, *126*(2), e2020JD033733. https://doi.org/10.1029/2020jd033733

Zhao, Y., Zhou, T., Li, P., Furtado, K., & Zou, L. (2021). Added value of a convection permitting model in simulating atmospheric water cycle over the Asian water tower. *Journal of Geophysical Research: Atmospheres*, *126*(13), e2021JD034788. https://doi.org/10.1029/2021jd034788

Zhou, P., Shao, M., Ma, M., Ou, T., & Tang, J. (2023). WRF gray-zone dynamical downscaling over the Tibetan Plateau during 1999–2019: Model performance and added value. *Climate Dynamics*, *61*(3–4), 1371–1390. https://doi.org/10.1007/s00382-022-06631-4